Computational Materials Science 81 (2014) 446–452

Contents lists available at ScienceDirect

Computational Materials Science

journal homepage: www.elsevier.com/locate/commatsci

Pseudopotentials for high-throughput DFT calculations

Kevin F. Garrity *, Joseph W. Bennett, Karin M. Rabe, David Vanderbilt

Department of Physics & Astronomy, Rutgers University, Piscataway, NJ 08854-8019, USA

ARTICLE INFO

Article history:
Received 5 July 2013
Received in revised form 23 August 2013
Accepted 25 August 2013
Available online 23 September 2013

Keywords:
Pseudopotentials
High-throughput
Density functional theory

ABSTRACT

The increasing use of high-throughput density-functional theory (DFT) calculations in the computational design and optimization of materials requires the availability of a comprehensive set of soft and transferable pseudopotentials. Here we present design criteria and testing results for a new open-source "GBRV" ultrasoft pseudopotential library that has been optimized for use in high-throughput DFT calculations. We benchmark the GBRV potentials, as well as two other pseudopotential sets available in the literature, to all-electron calculations in order to validate their accuracy. The results allow us to draw conclusions about the accuracy of modern pseudopotentials in a variety of chemical environments.

1. Introduction

The use of pseudopotentials for practical and efficient electronic-structure calculations has a long history in computational condensed-matter physics [1–5]. In pseudopotential-based electronic structure calculations, the nuclear potential and core electrons of an atom are replaced by a much softer effective potential felt by the valence electrons, enabling the latter to be described with a relatively small number of basis functions. Thus, the success and popularity of various first-principles density-functional theory [6,7] (DFT) codes using plane-wave basis sets (e.g. VASP [8,9], QUANTUM-ESPRESSO [10], ABINIT [11]) depend on the availability of high-quality pseudopotentials. While the publication and testing of entire pseudopotential libraries also has a long history [12–16], the dominant mode of pseudopotential design and testing has been that of case-by-case construction, with authors typically creating and testing potentials only for a specific application. This *ad hoc* method of pseudopotential design and testing is incompatible with the increasing use of first-principles DFT calculations in materials design applications, especially those that make use of high-throughput calculations to explore the properties of (possibly hypothetical) materials constructed from atoms across the periodic table [17–29]. Moreover, the pseudopotentials themselves (or the input data needed to construct them) are often not posted or published, and it is even more rare for comprehensive pseudopotential testing data to be made publicly available. Unfortunately, this state of affairs creates practical difficulties in the duplication of previous studies and limits our understanding of the accuracy and transferability of modern pseudopotentials in realistic calculations. In addition, the lack of an open-source pseudopotential library appropriate for high-quality high-throughput calculations likely limits the adoption of this technique.

In this work we introduce a new "GBRV" open-source pseudopotential library, explaining the design criteria used to construct it and providing a suite of test results to verify its accuracy. The GBRV library, available at http://physics.rutgers.edu/gbrv, consists of highly accurate ultrasoft [30] pseudopotentials generated using the Vanderbilt pseudopotential generation code [31]. We provide input files for the pseudopotential generator as well as ultrasoft pseudopotential files which can be used directly with QUANTUM ESPRESSO and projector-augmented wave (PAW) [32] files generated with the uspp2abinit [33] add-on which can be used directly with ABINIT. Our library has been designed and optimized for use in high-throughput DFT calculations, though it should be appropriate for many applications. In addition, we test two other PAW libraries, the mature but proprietary VASP PAW library version 5.2 [34] and the still-under-development PSLIB 0.3.0 public PAW library [35,36] generated using the ATOMIC code of the QUANTUM ESPRESSO package. Versions of the VASP library have been used in the majority of previous pseudopotential-based high-throughput studies, usually with little discussion of its accuracy [18–21,17,24,23,25,29].

Testing three potential sets allows us to assess the accuracy of our library relative to other choices and also provides some perspective on the limits of current pseudopotential methodology. We have tested the potentials by comparing with all-electron (AE) results from WIEN2k [37], which uses the highly accurate full-potential linearized augmented plane-wave + local orbitals method (FLAPW + LO).

The manuscript is organized as follows. Our pseudopotential design criteria are presented and discussed in Section 2. The tests

* Corresponding author. Tel.: +1 7812648936.
E-mail address: kgarrity@physics.rutgers.edu (K.F. Garrity).

0927-0256/$ - see front matter © 2013 Elsevier B.V. All rights reserved.
http://dx.doi.org/10.1016/j.commatsci.2013.08.053

of the GBRV, VASP and PSLIB potentials in comparison with AE calculations are presented in Section 3. Our conclusions are summarized in Section 4.

2. Pseudopotential design

2.1. Design criteria for high-throughput

High-throughput DFT studies of materials systems present a variety of challenges for pseudopotential design which have informed our choices in creating the GBRV pseudopotential library. First, by their very nature, high-throughput calculations include a wide variety of atoms and thus require accurate potentials extending throughout the periodic table. Therefore, our library includes all of the elements from H to Bi except for the noble gases and the *f*-block elements.

Second, high-throughput calculations require significant computational resources, which should be minimized if possible. Therefore, we designed our potential library so that all of the elements can be run at a relatively low plane-wave cutoff of 40 Ry and a charge-density cutoff of 200 Ry. Using a single low cutoff greatly simplifies the use of our potentials in high-throughput calculations. This contrasts with the normal procedure of allowing a variety of plane-wave cutoffs in a single pseudopotential library. In that case, one either has to use the highest cutoff in all calculations or else face difficulty in comparing energies of structures containing different combinations of atoms, a procedure that is central to the kind of thermodynamic stability analysis that is often required in high-throughput calculations.

Third, high-throughput calculations often place atoms in unusual or novel chemical environments. Therefore, we required that our potentials be highly transferable and able to reproduce metallic, ionic, and covalent bonding behavior. For the purposes of reliable high-throughput calculations, it is crucial that the potential library produces consistently accurate results for all atoms in all reasonable crystal structures. This requirement led us to include extra semi-core states in normally borderline cases, as a high-throughput study cannot verify whether the semicore states are necessary in every structure examined.

Finally, on a more technical level, high-throughput calculations of bulk materials typically require the use of variable unit-cell relaxation algorithms to minimize the stress and optimize lattice parameters. These calculations present numerical difficulties as they are normally run at a fixed number of plane-waves determined by the initial configuration, rather than at a fixed plane-wave cutoff, and they require accurate determination of stresses, which can be expensive to converge. Therefore, we designed our potentials such that when used with a smeared plane-wave cutoff they both produce accurate stresses and converge to an accurate ground state structure when using a variable cell relaxation algorithm (given a reasonable starting structure).

2.2. Pseudopotential construction

Unfortunately, designing a set of pseudopotentials which meets all of the above requirements is very difficult, as the requirements are naturally in conflict with each other. Highly transferable potentials generally require high plane-wave cutoffs and many semi-core states, which is in direct conflict with the requirement of a low plane-wave cutoff. In addition, a comprehensive set of potentials is both more difficult to design with a single low plane-wave cutoff and allows for many chemical environments, making reliability difficult. Given these conflicts, one is naturally led to adopt either ultrasoft or PAW potentials, which can provide both higher transferability and lower plane-wave cutoffs than norm-conserving potentials. In the present work, we have chosen to design a library of ultrasoft pseudopotentials. We describe our procedure for optimizing potentials below; however, there remain atoms which are particularly difficult to pseudize given the above constraints, which we discuss further when we present our testing data in Section 3.3.

The process of construction of the potentials consisted of optimizing the following parameters: (a) a reference atomic configuration (neutral or slightly ionic), (b) the number of core and valence states, (c) the cutoff radii for each angular momentum channel, (d) a local potential and local cutoff radii, (e) the inner pseudization and non-linear core correction radii, and (f) the energies of any extra projectors [38]. We began our design by constructing initial potentials from previously-tested potentials if available, using periodic trends to fill in missing elements, and testing each atom first in *fcc* and *bcc* structures and then using the NaCl testing set (see Section 3.2). We found that expanding our testing to the perovskites and half-Heuslers required relatively little additional tuning. While the traditional transferability tests provided by pseudopotential generators, such as comparing the logarithmic derivatives to all-electron results and testing the pseudopotential in multiple atomic configurations, were helpful in narrowing the choices of parameters for our potentials, we found that these tests are rarely sufficient to design a potential which meets the competing goals of our design criteria.

The various parameters of our potentials were adjusted by hand with extensive use of solid-state testing to identify which atoms need improvement and which aspects of those potentials must be modified. When a potential performed poorly in tests, we first adjusted the outer cutoff radii by deciding if the potential was either too hard or too soft. A potential which is too hard will improve its performance when tested with higher plane-wave and charge-density cutoffs, and requires increasing the cutoff radii of the local potential or non-local projectors, while an excessively soft potential must be adjusted in the opposite direction. Cutoff radii tend to follow periodic trends, with radii decreasing as one moves right across a row and increasing as one moves down a column, although differences in numbers of semicore states complicates this relation.

If an element had poor testing results which were found to be insensitive to the projector cutoff radii, there were several other options which we considered. First, we added any additional relevant semicore states or a non-linear core correction if there was significant valence/core overlap. Second, we looked in detail at the logarithmic derivatives and adjusted the local potential and the energies of any extra projectors in order to improve agreement in the chemically relevant region. Almost all of our occupied angular momentum channels have at least two projectors, and a few with semi-core states have three. We found that potentials heavier than fluorine generally require a good description of the *d* channel and the bottom 1–2 rows of the periodic table require a reasonable description of the *f* channel, especially for atoms near La–Hf. Third, it was sometimes necessary to adjust the inner pseudoization radius; magnetic moments are often particularly sensitive to this parameter. For most elements, we were able to achieve potentials which met all of our requirements after a few revisions, and small changes in the parameters would not affect the testing results noticeably. For a few problematic elements (Li, Be, F, Na, Ni, Hf) we were forced to systematically vary and test certain parameters that were found to be particularly important in balancing the trade-off between accuracy and hardness. In some cases we also had to adjust the local potential or reference configuration in order to find a region of parameter space which met our requirements as closely as possible. Having a large solid state testing set was important to prevent over-fitting of these difficult cases to any particular property. We discuss some of these atoms further in Section 3.3.

3. Tests

In order to gauge the transferability of a general-purpose pseudopotential library, it is necessary to test the potentials in chemical environments that include ionic, covalent, and metallic bonding. For this purpose, we have chosen a testing regimen in which the pseudopotential calculations are compared not with experiment, but with all-electron calculations performed under conditions that are as identical as possible. This allows us to quantify the accuracy of the pseudopotentials themselves, isolated from any complications having to do with actual experimental conditions (finite temperature, zero-point motion, etc.) or with theoretical approximations that are common to both the pseudopotential and all-electron calculations.

Thus, our pseudopotential and all-electron calculations are always carried out with exactly the same choice of DFT exchange–correlation functional, the same k-point sets, and the same smearing temperature. The PBE exchange–correlation functional [39] was used throughout. Both the AE calculations and the pseudopotential constructions were scalar-relativistic [40], i.e., without spin–orbit interactions.[1] We ran all of our testing calculations as non-spin-polarized calculations, except for our calculation of the magnetic moments of the transition metal oxides, which we ran at the all-electron non-spin-polarized lattice constants.

In the same spirit, we can reduce the computational load associated with the test suite by making some common approximations that still allow systematic comparison. For example, we ran all of our calculations on an $8 \times 8 \times 8$ k-point density and with 0.002 Ry Fermi–Dirac smearing. We note that this k-point and temperature setting is not sufficient to fully converge many of the properties we calculate and, as stated above, the results should not be compared with experiment. However, by using the same setting for all calculations, we can nevertheless compare the results to each other on an equal footing.

3.1. Testing procedure

Calculations with the GBRV pseudopotential set were run using QUANTUM ESPRESSO at our target plane-wave cutoff of 40 Ry and a charge density cutoff of 200 Ry. The PSLIB set provides a variety of suggested plane-wave cutoffs which range up to 78 Ry, but most are below 50 Ry and we ran all calculations with a cutoff of 50 Ry and a charge density cutoff of 450 Ry, also using QUANTUM ESPRESSO. This lower-than-recommended cutoff may bias results against PSLIB, but we think a relatively low cutoff is appropriate given our goal of testing potentials for high-throughput applications.

VASP provides a variety of potentials for each atom; we chose the potentials with the largest number of semi-core states (we did not test the new 'GW' potentials). These potentials have cutoffs of up to 47 Ry, although most are below 40 Ry. For cases such as O and F which include soft, normal, and hard versions, we chose the normal version. We ran all VASP calculations using the 'high' precision setting, which increases the plane-wave cutoff 25% above the suggested values, which is necessary to converge the stress for variable cell calculations.

WIEN2K calculations were performed at $R_{MT}K_{MAX}$ values of 8–10 as necessary to converge the lattice constant. Calculations of lattice constants and bulk moduli proceeded by first performing a variable-cell relaxation with the GBRV pseudopotential set to generate an initial guess for the lattice constant, and then performing energy calculations with each of our testing sets at nine points from −1% to 1% of the initial guess and fitting the results to a parabola.

[1] WIEN2K treats core electrons fully-relativistically, while the pseudopotentials treat the core electrons scalar-relativistically [40], which may result in small systematic errors.

Table 1
Summary of pseudopotential testing results. All testing data is presented as either RMS errors relative to AE calculations or percent of lattice constants outside ±0.2%. Only compounds where all three pseudopotential sets converge are included in RMS errors.

Test	GBRV	VASP	PSLIB
fcc latt. const. (%)	0.14	0.13	0.36
bcc latt. const. (%)	0.15	0.13	0.28
fcc bulk modulus (%)	3.6	4.1	5.4
bcc bulk modulus (%)	5.3	4.6	7.1
fcc–bcc Energy (meV)	3.7	3.6	5.4
rock salt latt. const. (%)	0.13	0.15	0.21
Rock salt bulk modulus (%)	5.0	4.5	4.9
Rock salt mag. mom. (μ_B)	0.08	0.22	0.01
Perovskite latt. const. (%)	0.08	0.13	0.20
Perovskite bulk modulus (%)	5.5	6.1	7.7
Half-Heusler latt. const. (%)	0.11	0.14	0.13
Half-Heusler bulk modulus (%)	5.4	5.8	5.1
fcc latt. const. > ±0.2% (%)	9.8	9.8	26.2
bcc latt. const. > ±0.2% (%)	9.8	8.2	27.9
Rock salt latt. const. > ±0.2% (%)	7.8	14.3	26.6
Perovskite latt. const. > ±0.2% (%)	0.0	14.5	27.3
Half-Heusler latt. const. > ±0.2% (%)	3.6	15.2	13.6

3.2. Details of the testing sets

Our four testing sets all consist of cubic materials without free internal parameters in order to reduce the computational demands associated with structural relaxation. Our first testing set consists of each of the elements in simple *fcc* and *bcc* structures. This set was designed to test the potentials in a metallic bonding environment as well as to allow us to analyze each potential separately, although we note that for many elements these structures are highly unrealistic and represent very demanding test cases.[2] The second testing set consists of rock salt structures designed to test ionic bonding. Main group elements are paired to put both elements in preferred oxidation states; most of these structures are insulating. All of the transition metal elements, which often have multiple oxidation states, are paired with oxygen; many of these are metallic. The third testing set consists of members of the heavily-investigated perovskite family. This set also largely tests ionic bonding, but includes tests of elements in higher oxidation states than the rock salt structures. Finally, we test a large set of half-Heusler structures (MgAgAs structure type, space group $F\bar{4}3m$) [41,26]. Half-Heuslers display a complicated combination of ionic, covalent, and metallic bonding, and should give an indication of the accuracy of our potentials in a variety of realistic environments. Both half-Heuslers and perovskites were chosen for their simple structure and their common inclusion of elements from throughout the periodic table. We include almost ninety previously synthesized half-Heuslers plus additional hypothetical examples, bringing our half-Heusler test set to 138 compounds, which include all of the elements in our pseudopotential set except H and the halogens.

3.3. Results

In Table 1, we present summary data for the overall performance the three pseudopotential sets (see Supplementary materials for more details). Each line in the table summarizes either the root-mean-squared (RMS) error relative to the AE calculations for a given type of test (excluding any cases in which there was a

[2] We were unable to converge WIEN2K calculations of the *fcc* and *bcc* structures of N, P, or Hg.

convergence failure for any of the pseudopotentials), or the percentage of structures in the testing set which have lattice constants errors outside the range of ±0.2%. Given our goal of transferability and reliability across a wide variety of structures as well as across the periodic table, this last measure is important to assess the robustness of the pseudopotential sets, rather than focusing only on averaged results, as reliable results require every calculation to be accurate. In general, we find that all three sets perform well, with most lattice constants within 0.2% of the all-electron results, and most bulk moduli within 5%. In fact, for many materials the differences between the pseudopotentials and all-electron calculations are comparable to uncertainties in the all-electron results themselves. For the properties included in our testing set, the aggregate performance of the GBRV pseudopotential set is superior to the VASP PAW library, especially with regards to the robustness of results for structures containing multiple elements in covalent and ionic environments. Both the GBRV and VASP sets give better lattice constants than PSLIB, but the bulk modulii and energy differences are similar for all three testing sets. PSLIB gives highly accurate magnetic moments, while VASP has a few elements which give poor magnetic moments.

The results for all three sets are clearly superior to those for norm-conserving pseudopotential libraries such as the TM [13] and HGH [14] sets, despite having significantly softer plane-wave cutoffs. For example, Fig. 5 of Ref. [15] compares the performance of some of these older comprehensive norm-conserving libraries against a recently-developed "Bennett–Rappe" library, using a test of half-Heusler lattice constants similar to that shown in the penultimate line of Table 1. The RMS lattice constant errors of 2.3% and 2.8% for the TM and HGH sets respectively were reduced to only 0.76% for the Bennett–Rappe set, with some of the most significant improvements occurring for transition-metal elements; this probably approaches the limit of what can be achieved in a single-projector norm-conserving framework [42]. The results for the ultrasoft and PAW libraries in Table 1, however, provide a dramatic additional reduction to less than 0.15% RMS error.

Graphical representations for some of the tests reported in Table 1 are presented in Figs. 1–5 Interestingly, the largest average errors tend to be in the simplest compounds, especially the *fcc* and *bcc* structures, and we note that the lattice constant errors for these two structures are highly correlated with each other (the correlation coefficient between the *fcc* and *bcc* lattice constant errors for the GBRV potential set is 0.95). In most cases the elements with large errors in *fcc* and *bcc* lattice constants and bulk moduli tend to have similar errors for all three pseudopotential sets, which suggests that the errors are related to the frozen-core approximation or some aspect of the all-electron calculations rather than any specific problem with a specific potential. The worst performing potentials in this test tend to be from either the alkaline metals or the halides, both of which tend to underestimate lattice constants. F and Cl, as well as several other first row elements including Li and Be, can be improved by reducing the cutoff radii and accepting higher plane-wave and charge density cutoffs; however, our current potentials perform sufficiently well in most realistic compounds (see below). The errors in the lattice constants of Rb and Cl may be related to the frozen-core approximation, as the errors were consistent across all of the pseudopotentials we constructed for these elements. The errors in energy difference between the *fcc* and *bcc* structures, shown in Fig. 3, tend to be small and highly correlated across all three pseudopotential sets. We note that the largest errors tend to be for elements with a large energy separation between the two structures, and that all of the calculations agree on the more stable structure in all cases except for Pd, where the calculated AE energy difference is only −1.5 meV/atom.

All of the potentials show good overall performance on most compounds in the rock salt, perovskite, and half-Heusler testing sets, as shown in Figs. 4–6 (see also Supplementary materials). Apparently the ionic and covalent bonding of these compounds is relatively insensitive to either the frozen-core approximation or the details of pseudopotential construction, at least for carefully tested potentials. The GBRV potentials have the advantage that they show fewer "poor" cases (defined as those showing lattice constant errors exceeding ±0.2%), which makes them particularly useful for a robust high-throughput study.

The GBRV potentials perform very well in the ionic NaCl and perovskite structures, as shown in Figs. 4 and 5, with the most notable exceptions being HfO and $SrHfO_3$. Hf has a filled 4*f* orbital which overlaps strongly both spatially and energetically with the valence and semicore *s*, *p*, and *d* orbitals, and this 4*f* orbital would have to be included in any truly transferable Hf potential. Unfortunately, including such a localized orbital is impossible within our convergence criteria. In order to treat these technologically important oxides accurately, in the spirit of Ref. [43], we created a second Hf potential, generated to reproduce a Hf^{4+} ionic configuration. This potential gives improved performance in Hf oxides, as shown by the green square in Figs. 4 and 5; however, it gives poor performance for metallic Hf (e.g., +0.71% lattice constant error in the *fcc* structure) and the errors reported in Table 1 all refer to the standard Hf potential. The remaining large errors in the ionic testing sets mostly involve combinations of alkaline metals with halides (e.g., LiI or CsCl), which we already noted are difficult to pseudize.

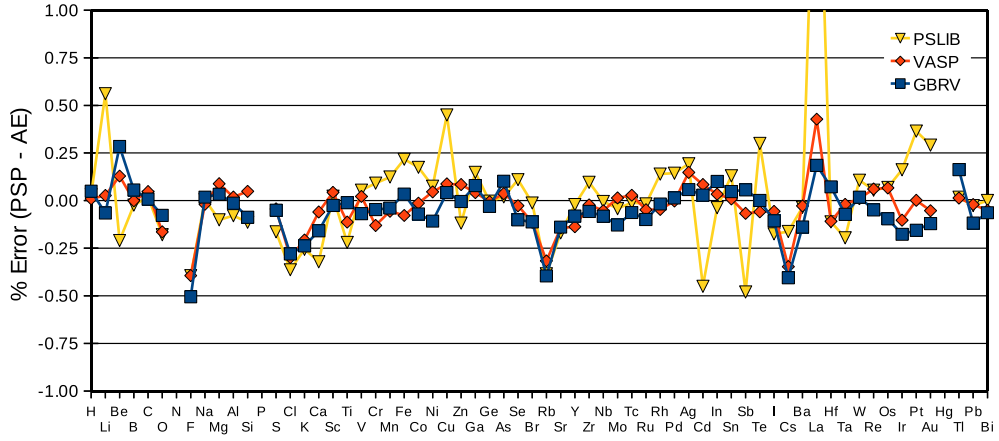

Fig. 1. Percent difference in AE versus pseudopotential calculations for *fcc* lattice constant. GBRV results in blue squares, VASP in red diamonds, and PSLIB potentials are yellow triangles. (For interpretation of the references to color in this figure legend, the reader is referred to the web version of this article.)

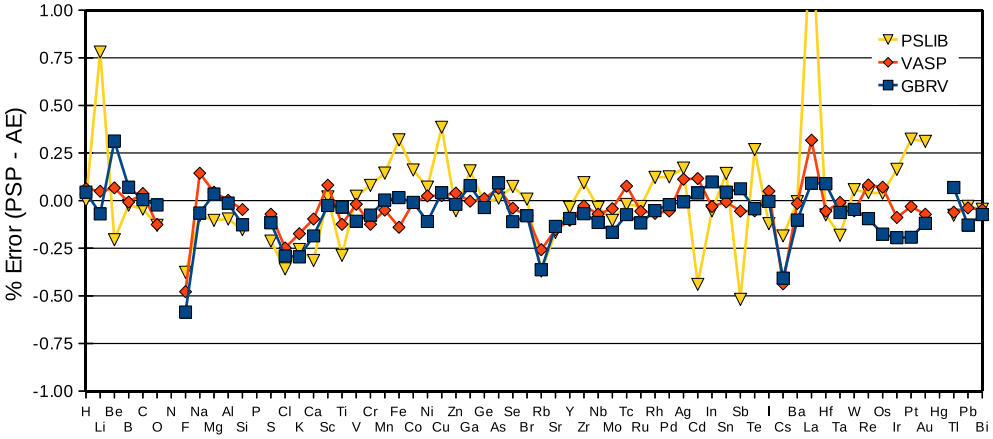

Fig. 2. Percent difference in AE versus pseudopotential calculations for *bcc* lattice constant. GBRV results in blue squares, VASP in red diamonds, and PSLIB potentials are yellow triangles. (For interpretation of the references to color in this figure legend, the reader is referred to the web version of this article.)

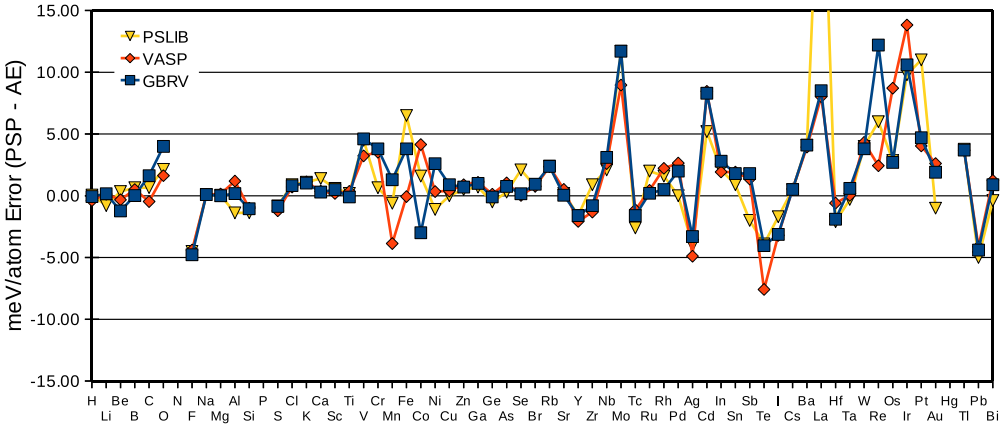

Fig. 3. Error in energy difference (meV per atom) between *fcc* and *bcc* structures. GBRV are in blue squares, VASP in red diamonds, and PSLIB in yellow triangles. For context, the standard deviation of the AE energy differences is 0.21 eV. (For interpretation of the references to color in this figure legend, the reader is referred to the web version of this article.)

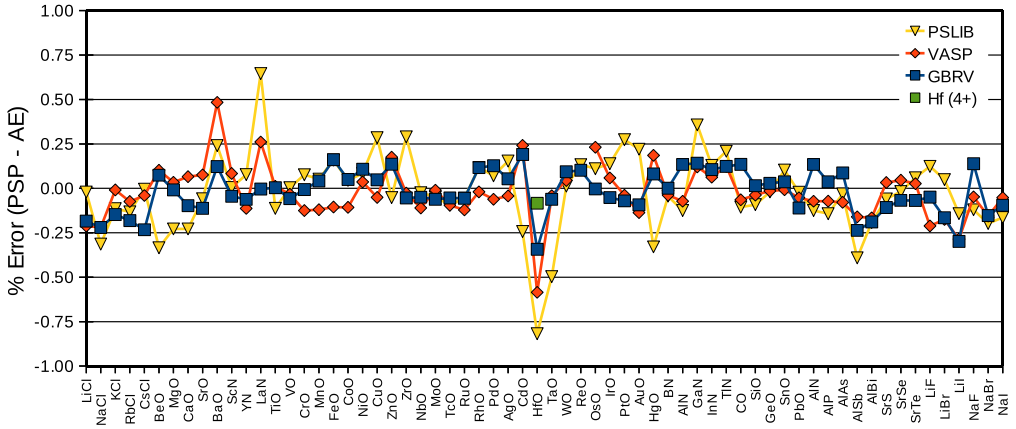

Fig. 4. Percent difference in AE versus pseudopotential calculations for rock salt lattice constants. GBRV potentials are blue squares, VASP potentials are red diamonds, PSLIB potentials are yellow triangles, and the Hf^{4+} potential is an isolated green square (see text). (For interpretation of the references to color in this figure legend, the reader is referred to the web version of this article.)

The performance of the GBRV potentials is also excellent for the large half-Heusler data set, as shown in Fig. 6. The lattice constant errors are approximately normally distributed, with a small bias of −0.07%, and only 5 out of 128 structures (SbTaCo, MnSbOs, MnPdTe, LiAuS, and CdPLi) outside of the ±0.2% lattice constant error range, and many of those barely outside. We note that the compounds with large errors all contain large transition metals, and that it is probably possible to improve Au, Cd, Pd, and Ta by including additional semicore states if more accuracy is required. The ability to modify potentials is an important feature of open-

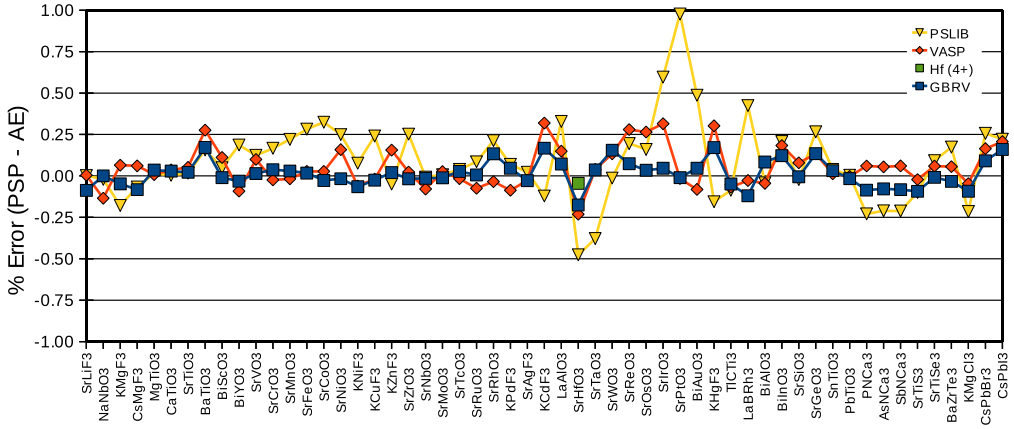

Fig. 5. Percent difference in AE versus pseudopotential calculations for perovskite (and anti-perovskite) lattice constants. GBRV potentials are blue squares, VASP potentials are red diamonds, PSLIB potentials are yellow triangles, and the Hf^{4+} potential is an isolated green square (see text). (For interpretation of the references to color in this figure legend, the reader is referred to the web version of this article.)

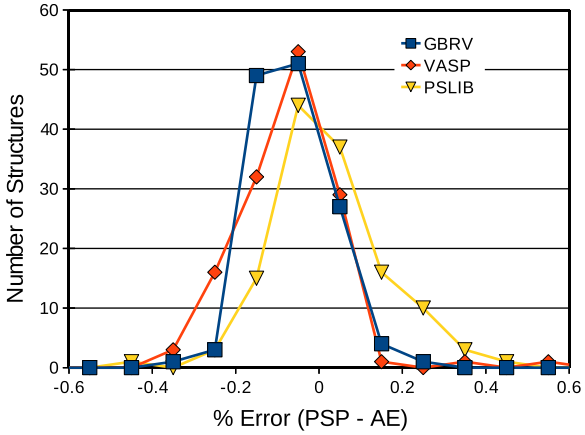

Fig. 6. Histogram of % error in lattice constants (PSP – AE) for the half-Heusler test set. GBRV results in blue squares, VASP in red diamonds, and PSLIB in yellow triangles. (For interpretation of the references to color in this figure legend, the reader is referred to the web version of this article.)

Table 2
Testing data for magnetic moments of transition metal oxides with non-zero magnetic moments at the AE non-spin polarized lattice constant. All magnetic moments in μ_B per primitive cell.

Compound	μ_{AE}	μ_{GBRV}	μ_{VASP}	μ_{PSLIB}
TiO	0.08	0.08	0.04	0.07
VO	1.55	1.54	1.44	1.55
CrO	2.91	2.98	2.97	2.90
MnO	3.83	3.90	3.84	3.82
FeO	3.83	3.85	3.83	3.83
CoO	2.59	2.78	2.69	2.59
NiO	1.82	1.75	1.01	1.83
MoO	0.42	0.43	0.42	0.42
TcO	2.02	2.01	2.01	2.02
RuO	1.44	1.43	1.45	1.44
RhO	0.36	0.36	0.37	0.36
ReO	0.11	0.11	0.09	0.11
OsO	1.79	1.79	1.79	1.79
IrO	0.79	0.80	0.79	0.79

source libraries such as GBRV. Fig. 6 also shows that the VASP and PSLIB potentials have tails of underestimated and overestimated lattice constants, respectively, which contribute to their higher RMS errors. Despite these outliers, we note that the remaining lattice constant errors are highly correlated across potential sets, with a correlation coefficient between the GBRV and VASP lattice constant errors of 0.63 (0.36 for GBRV and PSLIB). This correlation, which can also be seen in Figs. 1–5 for the previous testing sets, suggests that much of the remaining error is due to the frozen-core approximation. The errors in bulk modulus are even more highly correlated, with a correlation coefficient for the half-Heusler testing set of 0.92 between GBRV and VASP (0.84 between GBRV and PSLIB).

As a reminder, all the results presented until now have been for non-spin-polarized calculations. In order to obtain some information about the ability of the pseudopotentials to reproduce magnetic properties, we have carried out calculations for the binary transition-metal oxides in the rock salt structure (Fig. 4), but now initialized in a ferromagnetic spin configuration. For those that converged to a ferromagnetic ground state, we compare the resulting magnetic moments with the AE values in Table 2. (All four calculations agreed as to which materials remained ferromagnetic.) The PSLIB potentials reproduce the AE magnetic moments exceptionally well despite many elements having fewer semicore states than the other potential sets, which we attribute in part to their higher plane-wave and charge density cutoffs. The largest errors for the GBRV set are for NiO and CoO. We found that the magnetic properties of Ni in particular are very sensitive to its inner cutoff radius. Unfortunately, there is no value for this parameter which both reproduces the magnetic moment of NiO and is compatible with our convergence criteria; we had to compromise and choose the best value compatible with our requirements. We recommend significant testing before using any pseudopotential in detailed magnetic calculations.

The strong correlation between the lattice constant errors in the *fcc* and *bcc* structures, evident when comparing Figs. 1 and 2, suggests that it may be possible to create an estimate of the lattice constant error of other structures using this information. In other words, perhaps each element is consistently too small or too large across all structures, and this error can be corrected for. However, when we attempted to model the lattice constant errors of the GBRV potential set as a linear combination of the average *fcc* and *bcc* errors of the elements in each compound, we found little improvement in RMS errors beyond the improvement which came from subtracting the overall bias of −0.06%. Similarly, a model of the lattice constant error based on a global least squares fit to the testing sets, leaving out one compound at a time to evaluate the fit, improved RMS errors less than 0.01%. In other words, the bias introduced by each pseudopotential depends too strongly on chemical environment to be modeled with a single number.

Finally, note that we have been treating the AE results from WIEN2k as essentially exact, but this point deserves further investigation, as preliminary tests [44] indicate that the differences between different AE codes can sometimes be significant on the scale of our comparisons.

3.4. GBRV PAW library

In order to achieve broader compatibility with open-source electronic structure codes, specifically ABINIT, which can perform calculations with PAWs but not with ultrasoft pseudopotentials, we use the uspp2abinit [33] add-on to the Vanderbilt ultrasoft code to generate PAW versions of the GBRV library. While closely related, the formalism of PAW and ultrasoft potentials are not the same [34], which results in differences between the two GBRV potential sets which are larger than the differences between QUANTUM ESPRESSO and ABINIT when run with identical norm-conserving potentials. For some elements which are particularly sensitive to generation parameters, especially those with many semicore states or core states which are close in energy to valence states, we had to alter the generation parameters in order to make a PAW of equal accuracy to the ultrasoft version [45]. We find that the GBRV PAW and ultrasoft libraries, tested with ABINIT and QUANTUM ESPRESSO respectively, have the same overall accuracy relative to all-electron calculations, and their errors in lattice constant are highly correlated (e.g. the correlation coefficient between the perovskite lattice constant errors is 0.73).

4. Conclusions

In conclusion, we have presented design criteria and testing results for the new GBRV pseudopotential library optimized for high-throughput DFT calculations. We find that our potentials are both accurate and transferable, performing well in tests of metallic, ionic, and covalent bonding. In addition, we have compiled testing results for two PAW libraries, which also perform well and demonstrate the reliability of carefully designed pseudopotentials in electronic-structure calculations. While calculations using either ultrasoft pseudopotentials or PAWs are more complicated to implement than those using norm-conserving potentials, almost all modern electronic-structure codes are now capable of using such potentials, with current code development efforts continually expanding the set of features that are compatible with them. In particular, the GBRV potentials, available at http://physics.rutgers.edu/gbrv, can be used directly with the actively-developed open-source QUANTUM ESPRESSO and ABINIT packages.

For the properties investigated in this work, the GBRV potential set provides better accuracy and robustness than the VASP or PSLIB PAW sets, and at lower computational cost. In particular, the GBRV potentials are designed to run at a plane-wave cutoff of 40 Ry and a charge-density cutoff of 200 Ry, which are at least 25% lower than many of the PSLIB PAWs as well as lower than three VASP PAWs when using the 'high' precision setting recommended for variable cell relaxations.

The GBRV potentials (like the PSLIB potentials) also have the advantage of being open-source, which allows calculations to be easily replicated and enables the potentials to be modified and improved as needed by the electronic structure community. Furthermore, open-source potentials can be used with open-source electronic structure packages, which have active development communities and, like the potentials themselves, can be improved and expanded upon as necessary.

We hope that both the GBRV potential library itself, as well as the design criteria and testing methodology presented here, will improve the use and reliability of pseudopotential-based high-throughput DFT calculations for a variety of materials design applications.

Acknowledgements

This work was supported by NSF Grant DMR-10-05838 and ONR Grants N00014-09-1-0302 and N00014-12-1-1040. We wish to thank D.R. Hamann for valuable discussions.

Appendix A. Supplementary material

Supplementary data associated with this article can be found, in the online version, at http://dx.doi.org/10.1016/j.commatsci.2013.08.053.

References

[1] C. Herring, Phys. Rev. 57 (1940) 1169.
[2] J.C. Phillips, L. Kleinman, Phys. Rev. 116 (1959) 287.
[3] A. Zunger, M.L. Cohen, Phys. Rev. Lett. 41 (1978) 53.
[4] D.R. Hamann, Phys. Rev. Lett. 42 (1979) 662.
[5] D.R. Hamann, M. Schluter, C. Chiang, Phys. Rev. Lett. 43 (1979) 1494.
[6] P. Hohenberg, W. Kohn, Phys. Rev. 136 (1964) B864.
[7] W. Kohn, L. Sham, Phys. Rev. 140 (1965) A1133.
[8] G. Kresse, J. Hafner, Phys. Rev. B 47 (1993) R558.
[9] G. Kresse, J. Furthmuller, Phys. Rev. B 54 (1996) 11169.
[10] P. Giannozzi et al., J. Phys.: Condens. Matter 21 (2009) 395502.
[11] X. Gonze, G. Rignanese, M. Verstraete, J. Beuken, Y. Pouillon, R. Caracas, F. Jollet, M. Torrent, G. Zerah, M. Mikami, et al., Z. Kristall. 220 (2005) 558.
[12] G.B. Bachelet, D.R. Hamann, M. Schlüter, Phys. Rev. B 26 (1982) 4199.
[13] A. Khein, D. Allan, <http://www.abinit.org/downloads/psplinks/lda_tm_psp1_data>.
[14] C. Hartwigsen, S. Goedecker, J. Hutte, Phys. Rev. B 58 (1998) 3641.
[15] J.W. Bennett, Phys. Proc. 34 (2012) 14.
[16] K. Lejaeghere, V.V. Speybroeck, G.V. Oost, S. Cottenier, arXiv:1204.2733v3, 2012.
[17] A.R. Akbarzadeh, V. Ozoli, C. Wolverton, Adv. Mater. 19 (2007) 3233. ISSN 1521-4095.
[18] A. Jain, G. Hautier, C.J. Moore, S.P. Ong, C.C. Fischer, T. Mueller, K.A. Persson, G. Ceder, Comput. Mater. Sci. 50 (2011) 2295.
[19] G. Ceder, Y. Chiang, D. Sadoway, M. Aydinol, Y. Jang, B. Huang, Nature 392 (1998) 694.
[20] W. Setyawana, S. Curtarolo, Comput. Mater. Sci. 49 (2010) 299.
[21] S. Curtarolo, D. Morgan, G. Ceder, Calphad 29 (2005) 163. ISSN 0364-5916.
[22] G.H. Johannesson, T. Bligaard, A.V. Ruban, H.L. Skriver, K.W. Jacobsen, J.K. Norskov, Phys. Rev. Lett. 88 (2002) 255506.
[23] O. Levy, G.L.W. Hart, S. Curtarolo, J. Am. Chem. Soc. 132 (2010) 4830.
[24] D. Morgan, G. Ceder, S. Curtarolo, Meas. Sci. Technol. 16 (2005) 296. ISSN 0957-0233.
[25] S. Wang, Z. Wang, W. Setyawan, N. Mingo, S. Curtarolo, Phys. Rev. X 1 (2011) 021012.
[26] A. Roy, J.W. Bennett, K.M. Rabe, D. Vanderbilt, Phys. Rev. Lett. 109 (2012) 037602.
[27] J.W. Bennett, K.F. Garrity, K.M. Rabe, D. Vanderbilt, Phys. Rev. Lett. 109 (2012) 167602.
[28] J.W. Bennett, K.F. Garrity, K.M. Rabe, D. Vanderbilt, Phys. Rev. Lett. 110 (2013) 017603.
[29] X. Zhang, L. Yu, A. Zakutayev, A. Zunger, Adv. Funct. Mater. 22 (2012) 1425.
[30] D. Vanderbilt, Phys. Rev. B 41 (1990) 7892.
[31] http://www.physics.rutgers.edu/dhv/uspp/.
[32] P.E. Blöchl, Phys. Rev. B 50 (1994) 17953.
[33] M. Torrent, F. Jollet, <http://www.abinit.org/downloads/PAW2/USpp2Abinit-Manual-html/USppPAW2.htm>.
[34] G. Kresse, D. Joubert, Phys. Rev. B 59 (1999) 1758.
[35] http://www.qe-forge.org/gf/project/pslibrary/.
[36] X. Ge, B.I. Adetunji, M. Monni, E. Kucukbenli, A.D. Corso, S. de Gironcoli, Inter. Workshop on Comput. Phys. and Mater. Sci., Poster Abstract, 2013.
[37] K. Schwarz, P. Blaha, Comput. Mater. Sci. 28 (2003) 259.
[38] P. Giannozzi, Notes on pseudopotential generation, 2012. http://www.quantum-espresso.org/wp-content/uploads/Doc/pseudo-gen.pdf>.
[39] J.P. Perdew, K. Burke, M. Ernzerhof, Phys. Rev. Lett. 77 (1996) 3865.
[40] D. Koelling, B. Harmon, J. Phys. C: Solid State Phys. 10 (1977) 3107.
[41] T. Graf, C. Felser, S.S.P. Parkin, Prog. Solid State Chem. 39 (2011) 1.
[42] D.R. Hamann, Phys. Rev. B 88 (2013) 085117.
[43] S. Coh, T. Heeg, J. Haeni, M. Biegalski, J. Lettieri, L. Edge, K. O'Brien, M. Bernhagen, P. Reiche, R. Uecker, et al., Phys. Rev. B 82 (2010) 064101.
[44] G.-M. Rignanese, private communication.
[45] K.F. Garrity, Notes on abinit gbrv paws, 2013. http://www.physics.rutgers.edu/gbrv/notes_on_abinit3.pdf>.